THE JOURNAL OF PHYSICAL CHEMISTRY B
A JOURNAL OF THE AMERICAN CHEMICAL SOCIETY

pubs.acs.org/JPCB

Article

Cylindrical Confinement of Nanocolloidal Cholesteric Liquid Crystal

Published as part of The Journal of Physical Chemistry virtual special issue "125 Years of The Journal of Physical Chemistry".

Elisabeth Prince,[▽] Yongliang Wang,[▽] Ivan I. Smalyukh, and Eugenia Kumacheva*

Cite This: https://doi.org/10.1021/acs.jpcb.1c04387

Read Online

ACCESS | Metrics & More | Article Recommendations | Supporting Information

ABSTRACT: The organization of nanocolloidal liquid crystals in constrained geometries has fundamental and practical importance, since under confinement, liquid crystals contain stable topological defects that can serve as templates for nanoparticle organization. Three-dimensional confinement of cholesteric (Ch) liquid crystals formed by cellulose nanocrystals (CNCs) have been extensively studied; however, their two-dimensional confinement remains under-investigated. Here, we report the results of systematic experimental studies of two-dimensional confinement of Ch−CNC liquid crystal in cylindrical capillaries with varying inner diameters. Confinement resulted in phase separation of the Ch−CNC liquid crystal into a Ch shell formed by concentric CNC pseudolayers with the helicoidal axis perpendicular to the inner surface of the capillary walls, and a micrometer-diameter isotropic core thread running parallel to the long axis of the capillary. The morphology of the confined Ch−CNC liquid crystal varied when progressively increasing the degree confinement. Finally, we show that phase separation of the Ch−CNC liquid crystal into a Ch shell and an isotropic core is preserved in flexible capillary tubing, suggesting the applicability of this system for the fabrication of flexible optical waveguides.

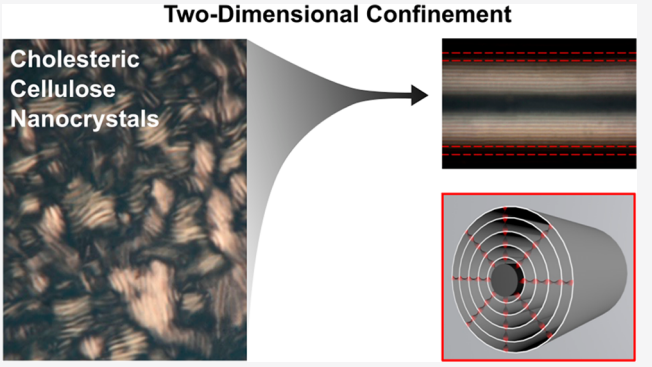

INTRODUCTION

Studies on the geometric confinement of nanoparticles (NPs), molecules, and liquid crystals are of fundamental and practical importance in the soft matter field. In particular, one-, two-, or three-dimensional confinement of liquid crystals breaks the symmetry of their equilibrium states and stabilizes topological defects (representing distorted regions of the director), thus giving rise to novel structures and patterns.[1,2] Two-dimensional confinement of liquid crystals in narrow capillaries[2,3] and three-dimensional confinement in spherical droplets[4,5] have given rise to new modes of packing, self-assembly, and phase separation, with promising applications of those assemblies in optics[6,7] and sensing.[8,9] Furthermore, confinement can provide insight into the self-assembly that occurs in biological liquid crystalline systems such as the cornea[10,11] and the exoskeleton of insects.[12,13]

Confinement of nanocolloidal liquid crystals, as opposed to molecular mesogens, may pave the way for designing new materials.[14,15] Micrometer-sized topological defects in nanocolloidal liquid crystals can compartmentalize guest NPs, thereby precisely directing their organization in three-dimensional space.[16−19] In addition, NP-laden droplets of colloidal liquid crystals exhibit interactive morphogenesis, with not only the liquid crystal directing self-assembly of NP guests but also the guest NPs altering the morphology of the liquid crystal host.[19] Notably, the self-assembled structures are not solely governed by the confinement geometry but are also dependent on the NP shape and surface chemistry.[16]

Rod-shaped cellulose nanocrystals (CNCs) have attracted immense interest from the research community, which is largely due to the formation of a cholesteric (Ch) liquid crystal by aqueous CNC suspensions.[20,21] It has been established that three-dimensional confinement of Ch−CNC suspensions in spherical droplets strongly impacts the morphology of the liquid crystal.[17−19,22−25] For example, Ch−CNC droplets with diameter of ∼90 μm had a core−shell structure with an isotropic core and a Ch shell, with CNCs forming concentric pseudolayers parallel to the droplet interface with a continuous phase. With droplet diameter reducing below 20 μm, the confined Ch−CNC phase adopted a bipolar planar morphology.[17] Latex, gold, carbon and magnetic NPs segregated in the topological defects in Ch−CNC droplets, that is, in the isotropic core and disclinations.[17,18] While three-dimensional confine-

Received: May 18, 2021
Revised: June 24, 2021

ment of nanocolloidal Ch−CNC liquid crystals has been explored, reports on their two-dimensional confinement remain scarce. Notably, by analogy with the results of studies of molecular mesogens, confinement of nanocolloidal liquid crystals in narrow capillaries can be used for the investigation of their relaxation dynamics, the formation of defects,[26,27] assembly of NPs,[3] and for applications in optics as low-loss waveguides.[28−32] A study of the confinement and drying of the CNC suspension in capillaries with a rectangular (50 × 1000 μm) cross-section revealed the formation of a monodomain crystalline film.[33] In a second study, confinement of CNC suspension in capillaries with a circular cross-section was used to study the relaxation dynamics of Ch−CNC liquid crystal.[27] A systematic investigation of how the degree of confinement influences the assembly of the Ch−CNCs is still lacking.

Here we report an experimental study of cylindrical, two-dimensional confinement of the nanocolloidal Ch−CNC liquid crystal. We show that upon confinement of the Ch−CNC liquid crystal in a narrow capillary, it undergoes phase separation into a Ch shell formed by concentric pseudolayers of Ch−CNCs with a helicoidal axis perpendicular to the capillary wall and a micrometer-diameter isotropic core thread that runs parallel to the long axis of the capillary. To explore the impact of the degree of confinement on CNC organization, we generated a "confinement gradient" by introducing a Ch−CNC liquid crystal in a capillary with a tapered geometry. Finally, we show that confinement-induced phase separation of Ch−CNC liquid crystal into an isotropic core thread and a Ch shell is preserved in flexible tubing, thus paving the way for the generation of flexible waveguides.

MATERIALS AND METHODS

Materials. An aqueous 12.2 wt % CNC suspension was purchased from the University of Maine Process Development Centre. Fluoresbrite YG carboxylated dispersions of 243 nm-size latex NPs were purchased from Polysciences, Inc., and microscopy immersion oil was purchased from Sigma-Aldrich Canada. Borosilicate glass capillaries were purchased from Hampton Research (inner diameter of 100 μm) and Sutter Instruments (inner diameter 900 μm). Teflon tubing with an inner diameter of 327 μm (catalog # 58698-U) was purchased from Sigma-Aldrich Canada.

Confinement Experiments. A 4.0 wt % CNC suspension was equilibrated for 7 days until it phase-separated into a top isotropic phase and a bottom Ch phase. The Ch-phase with CNC concentration of 4.16 wt % was separated from the isotropic phase and introduced into a borosilicate glass capillary with an inner diameter of 100 μm (HR6−104, Hampton Research) at a flow rate of 0.15 mL h^{-1} using a syringe pump (Harvard Apparatus). The capillary was then sealed with Duco cement and equilibrated in a horizontal position for at least 10 days.

In order to generate a gradient in the degree of confinement of Ch−CNC liquid crystal, capillaries with a tapered geometry were prepared. Fire polished borosilicate glass pipettes (Sutter Instruments) were loaded into a P1000 Micropipette Puller (Sutter Instruments). The following settings were used to generate tapered capillaries with inner diameter in the range from 1000 to 2 μm: heat ramp +30, pull 20, velocity 150, time 200, pressure 200 psi. The tips of the capillaries were fractured to obtain a tip inner diameter >20 μm, so that the viscous Ch−CNC suspension could be introduced into the capillary. A 4.16 wt % suspension of Ch−CNCs was loaded through the wider end of the capillary at a velocity of 0.15 mL h^{-1} and both ends were sealed with Duco cement.

To introduce the Ch−CNC liquid crystal into flexible Teflon tubing, the 4.16 wt % Ch−CNC suspension was introduced into the tubing at the flow rate of 0.15 mL h^{-1}. Both ends of the tubing were sealed with Duco cement. The tubing was allowed to equilibrate for 7 days.

Polarized Optical Microscopy (POM). To characterize the morphology of the Ch−CNC liquid crystal confined to the capillary, we utilized an Olympus BX51 microscope in the transmission mode using crossed polarizers. The pitch of the Ch−CNC shell and the diameter of isotropic core were determined by image analysis of the POM images using ImageJ (NIH).

Polymerization of Ch−CNC/Monomer Suspension. The Ch−CNC suspension was mixed with a 2-hydroxyethyl acrylate monomer, a poly(ethylene glycol) diacrylate cross-linker (M_n = 5 kDa), and a photoinitiator (Irgacure 2959) and allowed to equilibrate for 7 days for phase separation into the isotropic and Ch phases. The recipe of this mixture is given in Table S1, Supporting Information. After completion of phase separation, the bottom Ch−CNC suspension containing polymerization precursors was separated and injected into the capillary at a flow rate of 0.15 mL h^{-1}. After equilibration for different time intervals, the capillaries were subjected to ultraviolet irradiation (20 mW/cm^2, λ = 365 nm) for 15 min. After polymerization, the capillaries equilibrated for another 96 h.

Segregation Fluorescent NPs in the Isotropic Core of Confined Ch−CNC Liquid Crystal. The fluorescein isothiocyanate (FITC) labeled 243-nm-diameter polystyrene latex NPs had an electrokinetic potential (ζ-potential) of −18 mV. The CNC suspension was mixed with a dispersion of latex NPs to give a final volume fraction of the NPs of $\phi_{NP} = 2.4 \times 10^{-3}$. Over 7 days of equilibration, the mixture of CNCs and latex NPs phase-separated into an isotropic top phase and a Ch bottom phase, both containing latex NPs. The bottom Ch−CNC liquid crystal was introduced into the capillary and equilibrated for 25 days. Confocal fluorescence microscopy was used to examine the distribution of latex NPs in the confined Ch−CNC liquid crystal.

RESULTS AND DISCUSSION

Phase Separation of Ch−CNC Liquid Crystal in the Capillary. The rod-like CNCs had average diameter and length of 18 and 185 nm, respectively (Figure S1, parts A and B, Supporting Information). Owing to the anionic sulfate half-ester groups on their surface,[20] the CNCs had a negative ζ-potential of −44.1 ± 5.8 mV. Polarized optical microscopy (POM) imaging of the Ch−CNC phase revealed a multidomain pattern with a characteristic stripe structure (Ch pseudolayers) of tactoids (Figure S2, Supporting Information).

The Ch−CNC liquid crystal was loaded into the capillary with an inner diameter of 100 μm and equilibrated for different time intervals. The morphology of the confined liquid crystal was examined using POM, with the polarizer and analyzer positioned at ±45° to the long axis of the capillary. Parts A and B of Figure 1 show the POM image of the Ch−CNC suspension in the plane located 50 μm from the inner capillary wall, that is, at the middle plane of the Ch−CNC thread, after 120-h equilibration, while Video S1 shows stacked POM images of the Ch−CNC thread at different focal planes. The image revealed phase separation of the Ch−CNC suspension into a Ch

https://doi.org/10.1021/acs.jpcb.1c04387
J. Phys. Chem. B XXXX, XXX, XXX−XXX

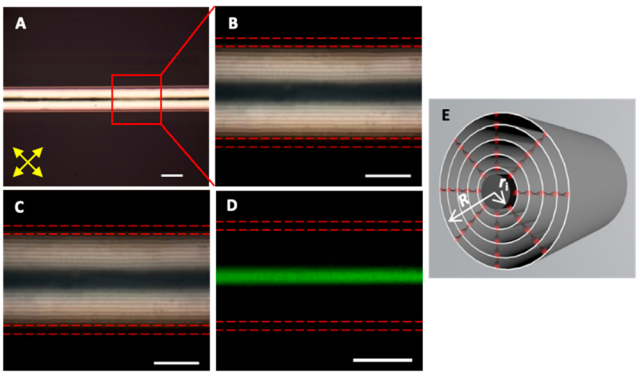

Figure 1. Confinement of Ch−CNC suspension in the capillary. (A, B) POM images of a 4.16 wt % Ch−CNC suspension confined to a 100 μm-diameter capillary after 120 h of equilibration, observed under low (A) and high (B) magnification. (C) POM images of the Ch−CNC suspension as in part B after 240 h of equilibration. Red dashed lines in parts B and C indicate the location of the capillary walls. (D) Confocal fluorescence microscopy image of the capillary filled with a mixture of Ch−CNC suspension with FITC-labeled polystyrene latex NPs ($\phi_{NP} = 2.38 \times 10^{-3}$). The green thread in the middle of the capillary represents fluorescent NPs partitioned in the central isotropic core (λ_{ex}= 488 nm). The dashed red lines outline the capillary walls. Scale bars in parts A−D are 100 μm. Yellow arrows in part A indicate the orientation of the polarizer and analyzer. (E) Schematic depicting 2D confinement of the Ch−CNC liquid crystal in the capillary. Red helicoids indicate the rotating director field.

shell and a dark isotropic core, with each phase forming a thread parallel to the long axis of the capillary. Under higher magnification, a characteristic striped structure of the Ch−CNC shell was observed, with pseudolayers of CNCs aligned parallel to the capillary wall surface. This core−shell morphology in the constrained directions was analogous to the structure observed for the Ch−CNC phase under spherical confinement in droplets, with concentric parallel pseudolayers forming a Ch shell around an isotropic core.[17] The average pitch of the Ch−CNC pseudolayers (defined as double the distance between the centers of two adjacent stripes) was 7.3 ± 0.3 μm (N = 50). The isotropic core had an average diameter, r_i, of 18.4 ± 1.3 μm (N = 50). The Ch−CNC morphology did not change over 240 h of equilibration of the Ch−CNC phase in the capillary (Figure 1C).

The existence of the isotropic core thread in the confined Ch−CNC suspension was further verified in several ways. First, we submerged the capillary filled with the Ch−CNC suspension in mineral oil with a refractive index of 1.51, that is, closely matching the refractive index of borosilicate glass of 1.52. The POM images of this system revealed the dark isotropic core thread and a Ch shell (Figure S3, Supporting Information). Second, by rotating the crossed polarizers (Figures S4 and S5 and Video S2, Supporting Information), we have verified that the central region is most commonly isotropic/disordered, rather than an unwound paranematic-like structure, albeit several Ch−CNC threads contained a paranematic central core, as we will discuss below. Finally, in several experiments, prior to introducing the Ch−CNC suspension into the capillary, we mixed it with fluorescent 243 nm-diameter polystyrene latex NPs with ζ−potential of −18 mV to give a final NP volume fraction of $\phi_{NP} = 2.38 \times 10^{-3}$. Notably, in previous studies, we have shown that addition of anionic 243-nm-diameter polystyrene NPs added to macroscopic suspensions of Ch−CNC suspensions to the concentration of $\phi_{NP} = 2.4 \times 10^{-2}$ does not disrupt the Ch structure.[17−19,34] Similar to the observations made for the Ch−CNC suspension confined to spherical droplets,[17−19] we observed partition of fluorescent latex NPs into the isotropic phase (the core thread), thereby forming a fluorescent strand in the center of the capillary (Figure 1D).

The images in Figure 1A−C correspond to an equilibrium structure under the confinement, with tangential boundary conditions for CNCs at the capillary wall surface, in marked difference with equilibrium flat pseudolayers generally observed for macroscopic Ch−CNC liquid crystals. The confinement leads to a radial orientation of the helical axis $\hat{\mathbf{h}}$, along which the

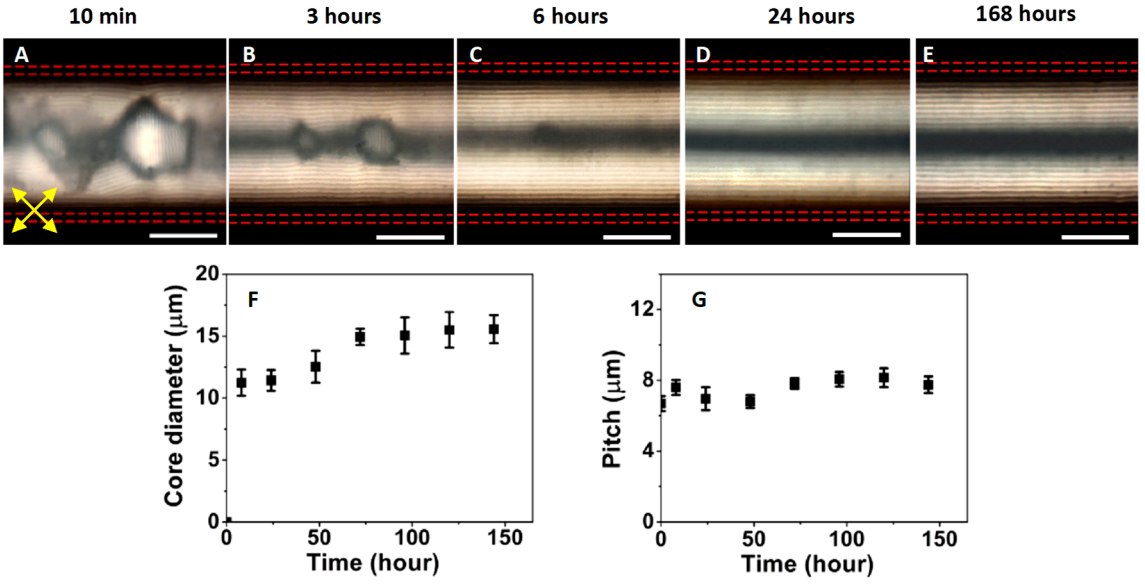

Figure 2. Evolution of Ch−CNC structure under two-dimensional confinement. (A−E) POM images of the Ch−CNC suspension equilibrated in the 100 μm-diameter capillary for different time intervals. Scale bars are 50 μm. Yellow arrows indicate the orientation of the polarizer and analyzer. (F) Temporal variation in the diameter of the isotropic core thread. (G) Temporal variation in pitch (double period) of the confined Ch−CNC phase.

https://doi.org/10.1021/acs.jpcb.1c04387
J. Phys. Chem. B XXXX, XXX, XXX−XXX

local orientation of the CNCs (described by the director field $\hat{\mathbf{n}}$ that is orthogonal to $\hat{\mathbf{h}}$) twists in space. Figure 1E shows a schematic of the cross-section of the Ch−CNC suspension under 2D confinement within the capillary. The inner diameter of the capillary is defined as R, while the diameter of the isotropic thread is defined as r_i. The red, twisted ribbon structures correspond to the twisted helicoidal director $\hat{\mathbf{n}}$, while the white concentric rings correspond to the bright regions of the pseudolayers in the POM images shown in Figure 1A−C. The dark gray region in the center of the cylinder depicts the disordered isotropic central part of the cylindrically confined Ch−CNC sample.

Evolution of the Core−Shell Structure of Ch−CNCs. The evolution of the "core−shell" morphology of the confined Ch−CNC liquid crystal was examined by POM during the equilibration time (Figure 2A−E). Immediately after introduction into a 100-μm-diameter capillary (Figure 2A), the Ch−CNC suspension exhibited a multidomain Ch structure with random $\hat{\mathbf{h}}$ and $\hat{\mathbf{n}}$ orientations. The evolution of the core−shell morphology occurred gradually, with multiple tactoids merging and changing the orientation of the director, until CNC pseudolayers were arranged parallel to the capillary walls. Within 3 h, dark regions emerged in the center of the capillary, and a characteristic striped structure of the Ch−CNC suspension appeared next to the capillary walls (Figure 2B). After 6 h of equilibration, a well-defined isotropic core thread evolved in the capillary center, which did not relax over at least, 168 h (Figure 2E). Figure 2F shows that the diameter of the isotropic core thread increased from 11.2 ± 1.1 to 15.6 ± 1.2 μm during 72 h of equilibration and subsequently did not change when examined at longer time intervals. The average pitch of the Ch−CNC structure was at 7.8 ± 0.5 μm over the entire equilibration time (Figure 2G). Polymerization vitrified confined Ch−CNC suspension after different time intervals of equilibration (Figure S6, Supporting Information).

The results shown in Figure 2 differ from the report on the relaxation of the core−shell morphology of the Ch−CNC thread under two-dimensional confinement in the capillary, that is, the disappearance of the dark core thread after 24 h through a transition from a paranematic-like unwound core to a Ch core.[27] Several key differences between our systems can lead to the different behavior of the confined CNC suspension. First, in our experiments, the concentration of the CNC suspension introduced in the capillary was 4.16 wt %, while a 2.7 wt % CNC suspension used in the previous work.[27] The higher concentration could result in higher elastic energy of the liquid crystal in the capillary center, thereby favoring the transition to the isotropic state and leading to slow relaxation.[17] We also note that the CNCs sources were different in two works, which could result in their different dimensions, surface chemistries, and charges, all of which could influence the formation of the isotropic phase and Ch phase with different pitches, relaxation dynamics, and the size and orientation of the Ch domains.[34,35]

Origin of the Axisymmetric Phase Separation. Cholesteric liquid crystals can exhibit structures with a nonsingular ordered central region in the form of the so-called λ^{+1}-disclination[21] and coaxial cylinder-shaped pseudolayers from the center to periphery of the capillary. In this case, the singularity in $\hat{\mathbf{n}}(\mathbf{r})$ can be avoided through the so-called "escape in the 3d dimension"[21] via axisymmetric twist, with $\hat{\mathbf{n}}(\mathbf{r})$ along the cylinder axis in its center. Our experiments, however, reveal that the Ch−CNC liquid crystal confined to the capillary tends to form an isotropic thread in the central region in the capillary core, which is surrounded by the Ch shell, as shown schematically in Figure 1E. To gain qualitative insights into the origin of this effect, we consider the elastic free energy under the conditions of such confinement (Figure 1). Within a coarse-grained model of Ch liquid crystals[21] and at a distance from the long axis at the capillary center larger than the pseudolayer thickness, the elastic free energy can be approximately expressed in terms of a gradient of the helical axis field, $\hat{\mathbf{h}}(\mathbf{r})$. Assuming that the contribution of the saddle-splay term can be neglected and that both the pseudolayer thickness and the density of CNCs remain constant, the free energy density can be expressed as $f_{el} = K_1(\mathrm{div}\ \hat{\mathbf{h}}(\mathbf{r}))^2/2$, where $K_1 = 3K_{33}/8$ is an elastic constant describing the energetic costs of splaying $\hat{\mathbf{h}}(\mathbf{r})$, expressed in terms of the Frank elastic constant K_{33} that is associated with the bend-type deformation of $\hat{\mathbf{n}}(\mathbf{r})$. The concentric arrangement of curved Ch pseudolayers shown in Figure 1A−C implies a radial configuration of $\hat{\mathbf{h}}(\mathbf{r})$, as shown in Figure 1E. By integrating f_{el} in a cylindrical coordinate system for the radial $\hat{\mathbf{h}}(\mathbf{r})$ observed in experiments (shown Figure 1E), one finds the elastic free energy per unit length of the capillary as $F_{el} = (3\pi K_{33}/8)\ln(R/r_i)$. Thus, toward the center of the capillary, the elastic energy increases because of the strong splay deformation of $\hat{\mathbf{h}}(\mathbf{r})$ and bend of $\hat{\mathbf{n}}(\mathbf{r})$. This increase in energy is consistent with our experimental results, as the central energetically costly region in the capillary center is replaced with the disordered phase (an isotropic core).

We admit that the formation of the dark region in POM images (shown in Figure 1A−C) could also correspond to the formation of a paranematic-like unwound region which replaced several Ch pseudolayers,[3] thus avoiding the strong curvature of these pseudolayers and strong bend-type deformations of $\hat{\mathbf{n}}(\mathbf{r})$ near the central region of the capillary. In this case, the isotropic vs. paranematic core regions could be distinguished based on the existence of a sharp interface between the isotropic domains and the paranematic regions in the capillary core, as we show in Figure 3A.

Effect of the Variation in the Degree of Confinement. To examine the limits in the formation of the linear isotropic core thread, we confined Ch−CNCs to capillaries with an inner diameter of 50 μm (Figure 3A, strong confinement) or 1200 μm (Figure 3B, weak confinement). Under strong confinement conditions, we observed the formation of nodes on the isotropic core thread with a diameter of 5.3 ± 0.4 μm, which were separated by the distance varying from 23 to 137 μm (Figure 3A). In contrast, under weak confinement, the Ch−CNC liquid crystal exhibited a multidomain structure (Figure 3B) that was characteristic for the unconfined Ch−CNC suspension, as shown in Figure S2, Supporting Information.

Close inspection of POM images of the Ch−CNC liquid crystal in the capillary with diameter of 50 μm revealed an interface between the paranematic phase and an isotropic phase (shown with arrows in Figure 3A, highlighted in the inset). The fact that the isotropic and paranematic phases in the central region of the capillary can coexist is not surprising, as they both arose to alleviate the frustration that would be otherwise caused by the strong curvature of Ch layers in the capillary center.

To examine the effect of the Ch−CNC liquid crystal confinement within these two extremes, we introduced the Ch−CNC suspension into a capillary with a tapered geometry, thereby producing a "confinement gradient." The Ch−CNC suspension was introduced in a capillary with a tapered geometry with an inner diameter varying from 94 to 900 μm, thereby producing a "confinement gradient". Figure 4A shows a brightfield image of the capillary with the tapered geometry.

https://doi.org/10.1021/acs.jpcb.1c04387
J. Phys. Chem. B XXXX, XXX, XXX−XXX

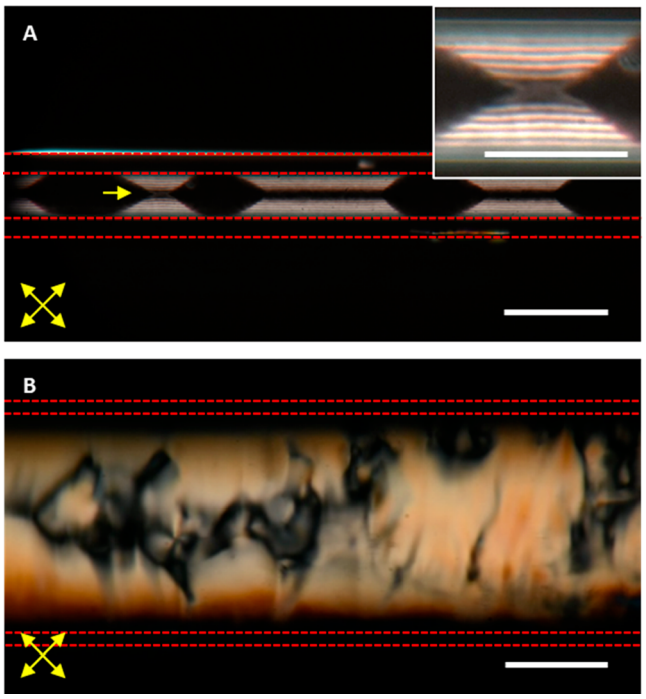

Figure 3. Limits in the confinement-induced separation of Ch−CNC liquid crystal. POM image of the confined Ch−CNC liquid crystal in the capillary with a diameter of 50 μm (A) and 1200 μm (B). Inset in part A shows a high magnification region that highlights the paranematic phase. Equilibration time was 7 days. Polarizer and analyzer are placed at ±45° with respect to the sample. The scale bar is 100 μm in part A, 50 μm in the inset, and 500 μm in part B. Yellow arrows indicate the orientation of the polarizer and analyzer.

High magnification POM images of regions with varying degrees of confinement are shown in Figure 4B, in which a dark and linear isotropic thread persisted in the capillary with a diameter of up to 445 μm. When the capillary diameter increased, the Ch shell became wider, as it contained more Ch pseudolayers. Interestingly, these added pseudolayers were angled away from the middle of the capillary to remain parallel to its inner walls. At the capillary diameter >870 μm, the Ch−CNC shell exhibited large defects. At the inner diameter of 900 μm, the core−shell morphology of the Ch−CNC thread was lost, and the confined suspension exhibited a multidomain structure.

The effect of confinement on the morphology of the confined Ch−CNC liquid crystal was characterized by examining the variation in pitch of the Ch shell, the number of pseudolayers in the Ch shell, and the volume fraction of the isotropic core. As the capillary diameter increased from 50 to 110 μm, the pitch increased from 7.0 ± 0.3 to 8.6 ± 0.4 μm (Figure 4C). Above a capillary diameter of 110 μm, the increase in pitch became more gradual; that is, it changed from 8.6 ± 0.4 to 9.1 ± 0.4 μm (Figure 4C). This result suggests that, under strong confinement, the Ch−CNC pseudolayers were compressed, while under weaker confinement, the pitch leveled off, approaching the value that was characteristic for the macroscopic Ch−CNC liquid crystal under equilibrium conditions. Furthermore, as the diameter of the capillary increased from 50 to 370 μm, the number of pseudolayers increased linearly from 14 to 75, indicating that they were continuously added through the edge dislocation defects, as is shown in Figure 4D. These edge dislocations are reminiscent of those formed in wedge-shaped cells with small dihedral angles.[35,36]

Notably, the volume fraction of the isotropic core, determined as $\phi_{core} = r_i^3/R^3 \times 100\%$, depended on the degree of confinement (Figure 4E). As R increased from 47 to 278 μm, ϕ_{core} decreased from 4.1 to 0.3%. This result is consistent with the effect of

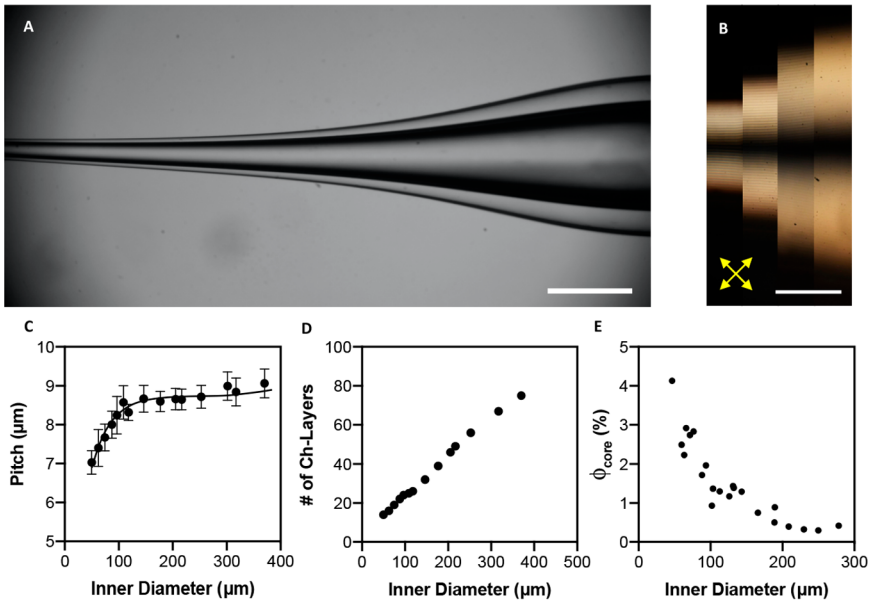

Figure 4. Impact of the degree of confinement on Ch−CNC structure. (A) Brightfield image of the tapered capillary showing the region with inner diameter changes varying from 94 to 685 μm. (B) Morphology of the Ch−CNC liquid crystal confined in the capillary with the tapered geometry. The inner diameter of the capillary changed from 130 μm (left) to 900 μm (right). Each fragment corresponds to a 58-μm-long section. The scale bar is 100 μm. Yellow arrows in part B indicate the orientation of the polarizer and analyzer. (C) Variation in the pitch of the confined Ch−CNC liquid crystal with the capillary diameter. Line is added for eye-guidance. (D) Variation in the number of Ch−CNC layers with the capillary diameter. (E) Variation in the volume fraction of the core, ϕ_{core}, vs. the capillary diameter.

https://doi.org/10.1021/acs.jpcb.1c04387
J. Phys. Chem. B XXXX, XXX, XXX−XXX

spherical confinement of Ch−CNC liquid crystal, where increasing confinement in smaller droplets resulted in an increase of the volume fraction of the isotropic core.[17]

Confinement of Ch−CNC Thread to Flexible Capillary. Being motivated by the utilization of confined nematic, smectic, and Ch liquid crystals as waveguides,[29,31,37] we introduced the Ch−CNC liquid crystal into a flexible Teflon tubing with an inner diameter of 327 μm and equilibrated it for 72 h. Subsequently, the tubing was bent with tweezers (Figure 5A).

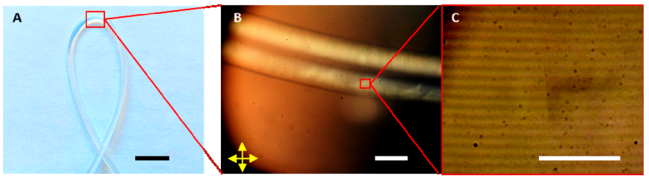

Figure 5. Ch−CNC-based flexible optical waveguide. (A) Photograph of the bent flexible Teflon tubing filled with Ch−CNC suspension. Scale bar is 1 mm. (B) POM image of the region highlighted in part A. Yellow arrows indicate the orientation of the polarizer and analyzer. Scale bar are 500 μm. (C) High magnification image of highlighted region in part B that reveals the Ch-pseudolayers. Scale bar is 25 μm.

Figure 5B shows a higher magnification image of the Ch−CNC thread in the tubing in Figure 5A submerged in a refractive index matching liquid (isopropyl alcohol/mixture water with an alcohol concentration of 70 v/v%). Notably, without the refractive index matching liquid, refraction at the air−Teflon tubing interface obscured visualization of the Ch−CNC structure; however, due to Teflon's crystallinity, the utilization of the solvent mixture did not completely compensate the visualization of the tubing walls. We note that the Teflon tubing is birefringent (Figure S7, Supporting Information), and thus the polarizer and analyzer had to be rotated to ±90° to observe the core−shell structure of the Ch−CNC thread. Figure 5B shows a POM image of the fragment of the confined Ch−CNC liquid crystal: an isotropic core thread in the center of the tubing, which was surrounded with a Ch−CNC shell (Figure 5, parts B and C).

The average pitch of the Ch-layers was 5.8 μm (N = 50), and the core diameter was 16 ± 3.5 μm (N = 50). In the tapered glass capillary at the same inner diameter (327 μm), the pitch was 9 μm (N = 50, Figure 4C), that is, substantially larger than the pitch observed in the flexible Teflon tubing. This difference can be attributed to the different surface energies of the walls of Teflon and glass. Notably, the isotropic core thread was curved with a radius of curvature of 4.9 mm, indicating that the adaptability of the Ch−CNC thread to flexible environments with curved geometries.

CONCLUSIONS

We investigated the organization of Ch−CNC nanocolloidal liquid crystal under two-dimensional confinement in narrow cylindrical capillaries. In the absence of confinement, Ch−CNCs form a liquid crystal with a mosaic pattern of multiple domains of flat, parallel pseudolayers and random orientation of the helicoidal axis of the director field, $\hat{\mathbf{h}}$ (Figure S2, Supporting Information).[35] Confinement in capillaries alters the Ch structure by curving the pseudolayers such that they arranged into concentric rings with a radial arrangement of $\hat{\mathbf{h}}$ (Figure 1E). The radial arrangement of $\hat{\mathbf{h}}$ leads to an increase in elastic energy in the capillary core, which resulted in axisymmetric phase-separation of the Ch−CNC liquid crystal into a Ch shell and an isotropic core, both spanning over the entire capillary length. The evolution of the core−shell morphology occurred by merging tactoid domains and changing the orientation of the director until the CNC pseudolayers were arranged parallel to the capillary walls. To examine how progressive confinement impacts the structure of the confined Ch−CNCs liquid crystal, we generated a "confinement gradient" by introducing it in the capillary with a tapered geometry. With decreasing capillary diameter (or increased degree of confinement), the pitch and the number of the pseudolayers reduced, and the volume fraction of the isotropic core increased.

Finally, we showed that the core−shell morphology of the confined Ch−CNCs is retained in flexible capillaries. Given that liquid crystalline phases are utilized as optical waveguides,[29,31,37] we propose that two-dimensional confinement of Ch−CNCs in flexible tubing could be used for the preparation of bendable waveguides. In addition to the potential application of the confined phase-separated Ch−CNC liquid crystal threads in optical devices, this work enhances our understanding of the role of confinement-induced organization of nanocolloidal liquid crystals.

ASSOCIATED CONTENT

Supporting Information

The Supporting Information is available free of charge at https://pubs.acs.org/doi/10.1021/acs.jpcb.1c04387.

Characteristics of cellulose nanocrystals, POM image of the macroscopic Ch−CNC suspension, POM images of the confined Ch−CNC liquid crystal, and POM image of Teflon tubing (PDF)

Video S1: stacked POM images of the Ch−CNC thread at different focal planes (MP4)

Video S2: confined Ch−CNC liquid crystal, rotating the polarizer while keeping the position of the analyzer constant (MP4)

AUTHOR INFORMATION

Corresponding Author

Eugenia Kumacheva − *Department of Chemistry, University of Toronto, Toronto, Ontario M5S 3H6, Canada; Department of Chemical Engineering and Applied Chemistry, University of Toronto, Toronto, Ontario M5S 3E5, Canada; Institute of Biomaterials and Biomedical Engineering, University of Toronto, Toronto, Ontario M5S 3G9, Canada;* orcid.org/0000-0001-5942-3890; Email: eugenia.kumacheva@utoronto.ca

Authors

Elisabeth Prince − *Department of Chemistry, University of Toronto, Toronto, Ontario M5S 3H6, Canada*

Yongliang Wang − *College of Materials Science and Engineering, Harbin University of Science and Technology, Harbin 150040, China*

Ivan I. Smalyukh − *Department of Physics and Soft Materials Research Center, University of Colorado, Boulder, Colorado 80309, United States; Materials Science and Engineering Program, University of Colorado, Boulder, Colorado 80309, United States;* orcid.org/0000-0003-3444-1966

Complete contact information is available at: https://pubs.acs.org/10.1021/acs.jpcb.1c04387

https://doi.org/10.1021/acs.jpcb.1c04387
J. Phys. Chem. B XXXX, XXX, XXX−XXX

Author Contributions

[▽]E.P. and Y.W. contributed equally.

Funding

This work was financially supported by the Natural Sciences and Engineering Research Council (NSERC) Canada via the Discovery and Canada Research Chair (Tier 1) programs and by the U.S. Department of Energy, Office of Basic 327 Energy Sciences, Division of Materials Sciences and Engineering, under Contract SC0019293 with the University of Colorado at Boulder. E.P. is grateful to NSERC for the Canada Graduate Scholarship-Doctoral Program. Y.W. expresses thanks for the support from the China Scholarship Council.

Notes

The authors declare no competing financial interest.

■ ACKNOWLEDGMENTS

Y.W. thanks Ms. Amanda Ackroyd for assistance in POM imaging and figure preparation and Prof. Yunfeng Li for useful discussions in the initial stage of the project.

■ ABBREVIATIONS

Ch; cholesteric; CNC; cellulose nanocrystals; POM; polarized optical microscopy.

■ REFERENCES

(1) Lavrentovich, O. D. Topological Defects in Dispersed Words and Worlds around Liquid Crystals, or Liquid Crystal Drops. *Liq. Cryst.* **1998**, *24* (1), 117−126.
(2) Nayani, K.; Chang, R.; Fu, J.; Ellis, P. W.; Fernandez-Nieves, A.; Park, J. O.; Srinivasarao, M. Spontaneous Emergence of Chirality in Achiral Lyotropic Chromonic Liquid Crystals Confined to Cylinders. *Nat. Commun.* **2015**, *6* (1), 8067.
(3) Kossyrev, P.; Ravnik, M.; Zumer, S. Branching of Colloidal Chains in Capillary-Confined Nematics. *Phys. Rev. Lett.* **2006**, *96* (4), 048301.
(4) Erdmann, J. H.; Zumer, S.; Doane, J. W. Configuration Transition in a Nematic Liquid Crystal Confined to a Small Spherical Cavity. *Phys. Rev. Lett.* **1990**, *64* (16), 1907−1910.
(5) Seč, D.; Porenta, T.; Ravnik, M.; Žumer, S. Geometrical Frustration of Chiral Ordering in Cholesteric Droplets. *Soft Matter* **2012**, *8* (48), 11982.
(6) Muševič, I. Liquid-Crystal Micro-Photonics. *Liq. Cryst. Rev.* **2016**, *4* (1), 1−34.
(7) Lee, S. S.; Seo, H. J.; Kim, Y. H.; Kim, S.-H. Structural Color Palettes of Core-Shell Photonic Ink Capsules Containing Cholesteric Liquid Crystals. *Adv. Mater.* **2017**, *29* (23), 1606894.
(8) Noh, J.; Henx, B.; Lagerwall, J. P. F. Taming Liquid Crystal Self-Assembly: The Multifaceted Response of Nematic and Smectic Shells to Polymerization. *Adv. Mater.* **2016**, *28* (46), 10170−10174.
(9) Popov, P.; Mann, E. K.; Jákli, A. Thermotropic Liquid Crystal Films for Biosensors and Beyond. *J. Mater. Chem. B* **2017**, *5* (26), 5061−5078.
(10) Rey, D. Liquid Crystal Models of Biological Materials and Processes. *Soft Matter* **2010**, *6*, 3402−3429.
(11) Busseron, E.; Ruff, Y.; Moulin, E.; Giuseppone, N. Supramolecular Self-Assemblies as Functional Nanomaterials. *Nanoscale* **2013**, *5* (16), 7098−7140.
(12) Seago, A. E.; Brady, P.; Vigneron, J.-P.; Schultz, T. D. Gold Bugs and beyond: A Review of Iridescence and Structural Colour Mechanisms in Beetles (Coleoptera). *J. R. Soc., Interface* **2009**, *6*, S165.
(13) Agez, G.; Bayon, C.; Mitov, M. Multiwavelength Micromirrors in the Cuticle of Scarab Beetle Chrysina Gloriosa. *Acta Biomater.* **2017**, *48*, 357−367.
(14) van Dommelen, R.; Fanzio, P.; Sasso, L. Surface Self-Assembly of Colloidal Crystals for Micro- and Nano-Patterning. *Adv. Colloid Interface Sci.* **2018**, *251*, 97−114.
(15) Smalyukh, I. I. Liquid Crystal Colloids. *Annu. Rev. Condens. Matter Phys.* **2018**, *9* (1), 207−226.
(16) Wang, D.; Hermes, M.; Kotni, R.; Wu, Y.; Tasios, N.; Liu, Y.; de Nijs, B.; van der Wee, E. B.; Murray, C. B.; Dijkstra, M.; et al. Interplay between Spherical Confinement and Particle Shape on the Self-Assembly of Rounded Cubes. *Nat. Commun.* **2018**, *9* (1), 2228.
(17) Li, Y.; Jun-Yan Suen, J.; Prince, E.; Larin, E. M.; Klinkova, A.; Thérien-Aubin, H.; Zhu, S.; Yang, B.; Helmy, A. S.; Lavrentovich, O. D.; et al. Colloidal Cholesteric Liquid Crystal in Spherical Confinement. *Nat. Commun.* **2016**, *7*, 12520.
(18) Li, Y.; Prince, E.; Cho, S.; Salari, A.; Mosaddeghian Golestani, Y.; Lavrentovich, O. D.; Kumacheva, E. Periodic Assembly of Nanoparticle Arrays in Disclinations of Cholesteric Liquid Crystals. *Proc. Natl. Acad. Sci. U. S. A.* **2017**, *114* (9), 2137−2142.
(19) Li, Y.; Khuu, N.; Prince, E.; Alizadehgiashi, M.; Galati, E.; Lavrentovich, O. D.; Kumacheva, E. Nanoparticle-Laden Droplets of Liquid Crystals: Interactive Morphogenesis and Dynamic Assembly. *Sci. Adv.* **2019**, *5* (7), eaav1035.
(20) Habibi, Y.; Lucia, L. A.; Rojas, O. J. Cellulose Nanocrystals: Chemistry, Self-Assembly, and Applications. *Chem. Rev.* **2010**, *110* (6), 3479−3500.
(21) Kleman, M.; Lavrentovich, O. D. *Soft Matter Physics*, 2003rd ed.; Partially Ordered Systems; Springer: New York, 2002.
(22) Parker, R. M.; Frka-Petesic, B.; Guidetti, G.; Kamita, G.; Consani, G.; Abell, C.; Vignolini, S. Hierarchical Self-Assembly of Cellulose Nanocrystals in a Confined Geometry. *ACS Nano* **2016**, *10* (9), 8443−8449.
(23) Wang, P.-X.; Hamad, W. Y.; MacLachlan, M. J. Polymer and Mesoporous Silica Microspheres with Chiral Nematic Order from Cellulose Nanocrystals. *Angew. Chem., Int. Ed.* **2016**, *55* (40), 12460−12464.
(24) Suzuki, T.; Li, Y.; Gevorkian, A.; Kumacheva, E. Compound Droplets Derived from a Cholesteric Suspension of Cellulose Nanocrystals. *Soft Matter* **2018**, *14* (47), 9713−9719.
(25) Cho, S.; Li, Y.; Seo, M.; Kumacheva, E. Nanofibrillar Stimulus-Responsive Cholesteric Microgels with Catalytic Properties. *Angew. Chem., Int. Ed.* **2016**, *55* (45), 14014−14018.
(26) Jeong, J.; Kang, L.; Davidson, Z. S.; Collings, P. J.; Lubensky, T. C.; Yodh, A. G. Chiral Structures from Achiral Liquid Crystals in Cylindrical Capillaries. *Proc. Natl. Acad. Sci. U. S. A.* **2015**, *112* (15), E1837−44.
(27) Khadem, S. A.; Bagnani, M.; Mezzenga, R.; Rey, A. D. Relaxation Dynamics in Bio-Colloidal Cholesteric Liquid Crystals Confined to Cylindrical Geometry. *Nat. Commun.* **2020**, *11* (1), 4616.
(28) Lo, S. K.; Galarneau, L. M.; Rogers, D. J.; Flom, S. R. Smectic Liquid Crystal Waveguides with Cylindrical Geometry. *Mol. Cryst. Liq. Cryst.* **1991**, *201* (1), 137−145.
(29) Whinnery, J.; Hu, C.; Kwon, Y. Liquid-Crystal Waveguides for Integrated Optics. *IEEE J. Quantum Electron.* **1977**, *13* (4), 262−267.
(30) Peccianti, M.; De Rossi, A.; Assanto, G.; De Luca, A.; Umeton, C.; Khoo, I. C. Electrically Assisted Self-Confinement and Waveguiding in Planar Nematic Liquid Crystal Cells. *Appl. Phys. Lett.* **2000**, *77* (1), 7−9.
(31) Zografopoulos, D. C.; Asquini, R.; Kriezis, E. E.; d'Alessandro, A.; Beccherelli, R. Guided-Wave Liquid-Crystal Photonics. *Lab Chip* **2012**, *12* (19), 3598−3610.
(32) Green, M.; Madden, S. J. Low Loss Nematic Liquid Crystal Cored Fiber Waveguides. *Appl. Opt.* **1989**, *28* (24), 5202−5203.
(33) Cherpak, V.; Korolovych, V. F.; Geryak, R.; Turiv, T.; Nepal, D.; Kelly, J.; Bunning, T. J.; Lavrentovich, O. D.; Heller, W. T.; Tsukruk, V. V. Robust Chiral Organization of Cellulose Nanocrystals in Capillary Confinement. *Nano Lett.* **2018**, *18* (11), 6770−6777.
(34) Thérien-Aubin, H.; Lukach, A.; Pitch, N.; Kumacheva, E. Structure and Properties of Composite Films Formed by Cellulose Nanocrystals and Charged Latex Nanoparticles. *Nanoscale* **2015**, *7* (15), 6612−6618.
(35) Schütz, C.; Bruckner, J. R.; Honorato-Rios, C.; Tosheva, Z.; Anyfantakis, M.; Lagerwall, J. P. F. From Equilibrium Liquid Crystal

https://doi.org/10.1021/acs.jpcb.1c04387
J. Phys. Chem. B XXXX, XXX, XXX−XXX

Formation and Kinetic Arrest to Photonic Bandgap Films Using Suspensions of Cellulose Nanocrystals. *Crystals* **2020**, *10* (3), 199.
(36) Kleman, M.; Lavrentovich, O. D. *Soft Matter Physics: An Introduction*; Springer: 2003.
(37) Kwon, Y. K.; Han, J. K.; Lee, J. M.; Ko, Y. S.; Oh, J. H.; Lee, H.-S.; Lee, E.-H. Organic−Inorganic Hybrid Materials for Flexible Optical Waveguide Applications. *J. Mater. Chem.* **2008**, *18* (5), 579−585.

https://doi.org/10.1021/acs.jpcb.1c04387
J. Phys. Chem. B XXXX, XXX, XXX−XXX